Research Article | Vol. 29, No. 14 / 5 July 2021 / Optics Express 22146
Optics EXPRESS

Impact of optical noises on unipolar-coded Brillouin optical time-domain analyzers

XIA GAO,[1,5] ZHISHENG YANG,[1,2,5,*] SHENG WANG,[1,3] XIAOBIN HONG,[1,6] XIZI SUN,[1] MARCELO A. SOTO,[4] JIAN WU,[1] AND LUC THÉVENAZ[2]

[1]*State Key Laboratory of Information Photonics & Optical Communications, Beijing University of Posts and Telecommunications, Beijing 100876, China*
[2]*Ecole Polytechnique Fédérale de Lausanne (EPFL), Group for Fiber Optics, SCI STI LT Station 11, 1015 Lausanne, Switzerland*
[3]*Beijing National Railway Research & Design Institute of Signal & Communication Group Co., Ltd. Beijing 100070, China*
[4]*Department of Electronics Engineering, Universidad Técnica Federico Santa María, Valparaíso, Chile*
[5]*These authors contribute equally to this work*
[6]*xbhong@bupt.edu.cn*
[*]*zhisheng.yang@bupt.edu.cn*

Abstract: Noise models for both single-pulse and coded Brillouin optical time-domain analyzers (BOTDA) are established to quantify the actual signal-to-noise ratio (SNR) enhancement provided by pulse coding at any fiber position and in any operating condition. Simulation and experimental results show that the polarization noise and spontaneous Brillouin scattering (SpBS) to signal beating noise could highly penalize the performance of coded-BOTDA, depending on the code type and the interrogated fiber position. The models also serve as a useful tool to optimize the SNR improvement by trading off the accumulated Brillouin gain and optical noises.

1. Introduction

Distributed optical fiber sensors based on Brillouin optical time-domain analysis (BOTDA) have attracted considerable attentions in recent years, owing to its capability to inform on the spatial distribution of targeted quantities over a long optical fiber (> 25 km) [1–4]. In any BOTDA system, the signal-to-noise ratio (SNR) on the sensor response scales and trades-off all critical sensing specifications [5], therefore any approach improving the SNR, i.e. increasing the signal and/or reducing the noise, can directly lead to an improved sensing performance. Over the last decade, the SNR of conventional single-pulse BOTDA has been optimized towards its physical limits. In an optimized BOTDA, the powers of the pump pulse and the probe wave are limited by nonlinear effects [6–10], while the minimum noise power is determined by the photodetector quality and the target spatial resolution [11].

One of the approaches to further enhance the SNR is the optical pulse coding technique, which launches one or several trains of pulses into the sensing fiber, exploiting code types such as Golay, Simplex, cyclic, genetic-optimized codes and their derivatives [12–19]. Mathematically, coding techniques operate by enhancing the pump energy without affecting the noise, such that after decoding the single-pulse response can be retrieved with a reduced noise level. In other words, the SNR improvement (so-called coding gain) provided by coding techniques is indeed the ratio of the noise levels before and after decoding, which is calculated to be proportional to square-root of the coding length [12–19]. Very importantly, such a coding gain can be fully achieved only if the noise level remains unchanged between coded- and single-pulse BOTDA schemes, generally meaning that only if the photo-detection thermal noise dominates the measurements. However, apart from the thermal noise, there are Brillouin-gain-dependent optical noises such as

#426655 https://doi.org/10.1364/OE.426655
Journal © 2021 Received 1 Apr 2021; revised 17 Jun 2021; accepted 20 Jun 2021; published 29 Jun 2021

Optics EXPRESS

polarization noise and spontaneous Brillouin scattering (SpBS) to signal beating noise [20,21], which may be considerably enhanced from single-pulse BOTDA to coded BOTDA due to the largely increased pump energy, penalizing the theoretical coding gain. In addition, the behavior of such noises and the resulting impact on the coding gain differs depending on the code type in use and the interrogated fiber position. All these aspects have not yet been clearly addressed in literature.

In this paper, aiming at fully evaluating the actual performance of coding techniques under a given experimental condition, noise models for single-pulse and coded-BOTDA are established and validated. The impact of optical noises on the performance of coded-BOTDA is studied for both periodic codes (e.g. cyclic codes [14]) and aperiodic codes (e.g. Golay [12], Simplex [13], and GO code [16]). Results demonstrate that, for aperiodic codes, at the fiber near-end, optical noises are far larger than the photo-detection thermal noise, so that the theoretical coding gain is largely compromised. The contribution of optical noises reduces with distance due to the fiber attenuation, resulting in a reduced penalty (even no penalty when the sensing fiber is considerably long) on the theoretical coding gain. However, for periodic codes, optical noises remain globally high and unchanged along the measured trace, affecting the entire sensing fiber length and penalizing the coding gain at all fiber positions.

2. Noise analysis of a single-pulse BOTDA system

The study starts by analyzing the impact of Brillouin-gain-dependent noises on a single-pulse BOTDA system. To be consistent with the analysis of coded-BOTDA in the next section, we here consider that a polarization scrambler is used to alleviate the polarization fading effect [22–24]. The noise model is established by assuming that the Brillouin frequency shift (BFS) profile of the sensing fiber is uniform, corresponding to the worst-case scenario, since the impact of additional Brillouin-gain dependent noises at the Brillouin gain peak is the most detrimental. In this case, the photocurrent of the detected optical signal (raw BOTDA trace) at the n^{th} single acquisition (non-averaged), converted into the distance domain using the light group velocity, can be expressed as:

$$I(z,n) = \eta P_S^0 \exp[g(z,n)] + e_{SpBS-S}(z,n) + e_{PD}(z,n), \tag{1}$$

where $\eta \approx 1$ A/W is the responsivity of the photodetector; P_S^0 is the power of the continuous component of the probe reaching the receiver; $e_{SpBS-S}(z,n)$ and $e_{PD}(z,n)$ denote photocurrents attributed to SpBS-signal beating noise and photodetection noise, respectively; $g(z,n)$ is the net Brillouin gain at resonance, which is practically affected by polarization fading and expressed as:

$$g(z,n) = 2\overline{g(z)}\cos^2\theta(z,n), \tag{2}$$

where $\overline{g(z)} = g(z,n)_n$ is the mean local Brillouin gain, averaged over all possible states of polarization n; $\theta(z,n)$ is the relative polarization angle between the pump pulse and probe wave at a fiber position z, and is given by a random value following a normal distribution in the range $[0,\pi]$ for each acquisition number n (when using a polarization scrambler). To retrieve $g(z,n)$ from the raw trace, a logarithmic normalization [23] should be applied to Eq. (1), resulting in:

$$\begin{aligned} g_{retrieved}(z,n) &= \ln\left[\frac{I(z,n)}{\eta P_S^0}\right] = \ln\left\{\exp[g(z,n)] + \frac{e_{SpBS-S}(z,n) + e_{PD}(z,n)}{\eta P_S^0}\right\} \\ &\approx g(z,n) + \frac{e_{SpBS-S}(z,n)}{\eta P_S^0 \exp[g(z,n)]} + \frac{e_{PD}(z,n)}{\eta P_S^0 \exp[g(z,n)]} \\ &\approx g(z,n) + \frac{e_{SpBS-S}(z,n)}{\eta P_S^0} + \frac{e_{PD}(z,n)}{\eta P_S^0}, \qquad \text{for } |g(z,n)| \ll 1. \end{aligned} \tag{3}$$

Optics EXPRESS

Note that a well-designed long-range BOTDA sensor must operate in small-gain regime, therefore the logarithm normalization is not normally performed due to the possible linearization of the exponential gain function. Under this condition, using $|g(z,n)| \ll 1$ also leads to the expression of Eq. (3). The retrieved gain is subject to 3 noise sources presented in the last row of Eq. (3), respectively:

1) *Polarization noise* (presented in $g(z,n)$ of Eq. (3)), which results from the polarization fading effect as described by Eq. (2) and can be characterized by its standard deviation (STD) as:

$$\sigma_{Pol}(z) = \sqrt{\langle g(z,n)^2 \rangle_n - \langle g(z,n) \rangle_n^2} = \frac{|\overline{g(z)}|}{\sqrt{2}}, \tag{4}$$

where the absolute value of gain is employed since $\overline{g(z)}$ is either positive (in Brillouin gain configuration) or negative (in Brillouin loss configuration). This $\sigma_{Pol}(z)$ represents the maximum possible STD of the local Brillouin gain variation caused by polarization fluctuations introduced by a scrambler. The actual STD at each fiber location is equal to or smaller than this value, as the optical fiber is a low-birefringent medium such that there exist sharp state of polarization (SOP) transitions over short fiber sections [25], partially or entirely averaging out polarization fluctuation effects within the pulse duration. In other words, at some fiber positions, no matter what the SOP of the pump pulse provided by the polarization scrambler is, it always shows a net Brillouin gain close to the mean local Brillouin gain $\overline{g(z)}$, corresponding to an STD much lower than the value expressed in Eq. (4). This phenomenon can be visualized in a single-pulse BOTDA system with a high Brillouin gain, in which the polarization noise is far larger than other noises, as exemplified in Fig. 1(a). The figure shows 20 non-averaged single-pulse Brillouin gain traces at resonance over a 2 km-fiber with the use of a polarization scrambler. To ensure a dominant polarization noise, a 20-ns pump pulse with 30 dBm peak power is used, resulting in a mean Brillouin gain $\bar{g} \approx 20\%$ at each fiber location (neglecting the fiber loss). It can be observed that the Brillouin gains at some fiber positions (e.g. at 0.21 km) among these 20 acquisitions are always close to $\bar{g}$ at any single acquisition, regardless of the polarization state of the pump pulse. This point has a very low STD due to local polarization noise, as shown in Fig. 1(b), while the maximum STD matches well with the theoretical value analytically calculated from Eq. (4). Such worst STD is the most representative, as the standard metric to qualify any distributed sensor is to evaluate the response at the lowest SNR position. It is also worth mentioning that, the detrimental impact of polarization noise can be greatly reduced if the polarization scrambler is replaced by a polarization switch; however, the use of the polarization scrambler is mainly discussed in this paper since it must be used for coded BOTDA to alleviate the polarization pulling effect [23].

2) *SpBS-Signal beating noise* (described by the term $e_{SpBS-S}(z,n)/(\eta P_S^0)$ in Eq. (3)), which results from the beating between the probe signal reaching the photodetector ($E_S(z)$) and the SpBS originating from the pump wave ($E_{SpBS}(z)$). The SpBS-signal beating noise STD can be expressed as [20,21]:

$$\sigma_{SpBS-S}(z) = \frac{\sqrt{E_{SpBS}^2(z) E_S^2(z)}}{P_S^0} = \sqrt{\frac{P_{SpBS}(z)}{P_S^0}} \propto \sqrt{\frac{|\overline{g(z)}|}{P_S^0}}, \tag{5}$$

where $P_{SpBS}(z) = \alpha_{SpBS} \Delta z P_P(z)$ is the SpBS power originating from the single pulse, which is proportional to the energy of the pump pulse $\Delta z P_P(z)$. Parameters α_{SpBS}, Δz, and $P_P(z)$ are the scattering coefficient of SpBS, spatial resolution and pulse power, respectively. $P_{SpBS}(z)$ is proportional to the energy of the pump pulse.

Optics EXPRESS

3) *Photo-detection noise* (described by the term $e_{PD}(z,n)/(\eta P_S^0)$ in Eq. (3)), which is usually dominated by the thermal noise due to the low power of the probe and the high transimpedance of the photodetector used [26]. The photo-detection noise STD can therefore be expressed as:

$$\sigma_{PD}(z) \approx \frac{\sigma_{th}}{\eta P_S^0}, \tag{6}$$

where σ_{th} is the thermal noise STD, which can be readily characterized by measuring the photodetector output without light input [21].

Equations (4), (5) and (6) indicate that the effects of SpBS-signal beating noise and thermal noise on the Brillouin gain calculation are inversely proportional to the probe power (P_S^0) reaching the receiver, while the polarization noise is irrelevant with respect to P_S^0. This verifies the fact that the probe power reaching the receiver should be always maximized to minimize the total equivalent noise [21]. On the other hand, for a given PD and P_S^0 (i.e. fixed equivalent thermal noise), the polarization noise and SpBS-signal beating noise are proportional to the mean local Brillouin gain $|\overline{g(z)}|$, with linear and square root relations, respectively. Figure 2 shows the calculated STD of each noise and total noise ($\sigma_{Total} = \sqrt{\sigma_{Pol}^2 + \sigma_{SpBS-S}^2 + \sigma_{PD}^2}$) as a function of $|\overline{g(z)}|$. In the calculation, P_S^0 is set to -20 dBm that matches the saturation power of the photodetector used in the experiment. It can be found that the thermal noise dominates when $|\overline{g(z)}|$ is small (< 1%, see inset figures in Fig. 2); as $|\overline{g(z)}|$ increases, the polarization noise rapidly grows and dominates, while the SpBS-signal beating noise always shows negligible contribution.

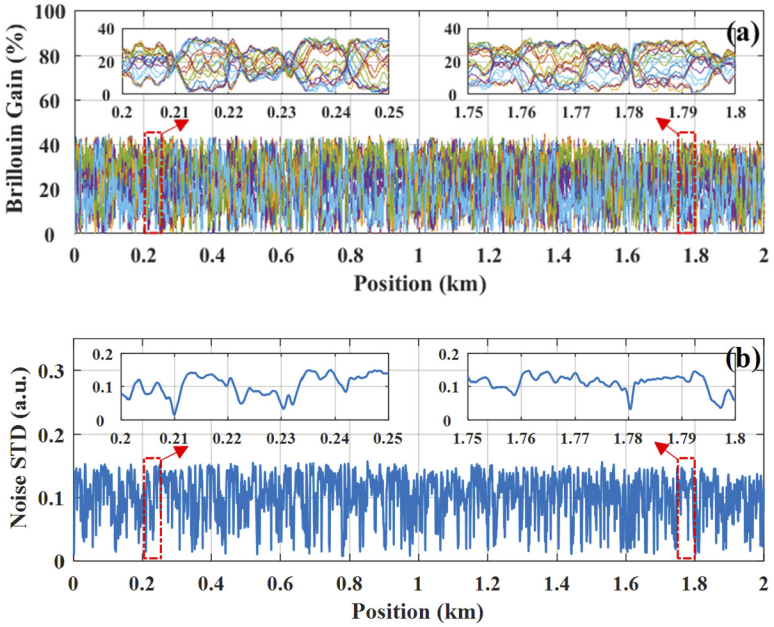

Fig. 1. (a) 20 consecutive single-pulse Brillouin gain traces obtained over a 2km-fiber without averaging at the resonance frequency. (b) STD of the corresponding local polarization noise. Both insets represent a zoom-in of the respective figures in the range from 0.2 km to 0.25 km distance (near the fiber input) and from 1.75 km to 1.8 km distance (near the fiber end).

The above analysis is verified by experimentally characterizing the noise at the Brillouin peak resonance over a 2-km sensing fiber (the same fiber used in Fig. 1). The power of the

Optics EXPRESS

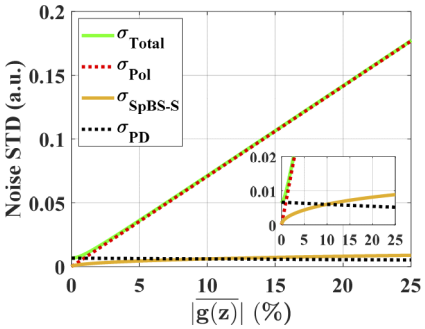

Fig. 2. STD of noises as a function of $|\overline{g(z)}|$. Simulation's parameters are: $P_S^0 = -20\ dBm$; $P_P = +20\ dbm$; $\alpha_{SpBS} = -93$ dB/m; The photodetector responsivity η and conversion gain are 1 A/W and 150000 V/A, respectively. The inset represents a zoom-in of Fig. 2 in the range of noise STD from 0 to 0.02.

probe light reaching the receiver is adjusted to -20 dBm (just below the PD saturation). The pump pulse width is set to be 20 ns, and for comparison, the pulse power is tuned to obtain four different mean Brillouin gains, i.e., $|\bar{g}| = 2.5\%$, 5%, 10% and 20%, respectively. Note that such high Brillouin gains can be reached thanks to the short fiber length (so a short effective nonlinear length). The corresponding noise STDs are shown in Fig. 3(a-d), respectively, based on 20 consecutive single-pulse Brillouin gain traces without averaging. The experimentally obtained noise STDs (blue curves) vary along the fiber as a result of the previously explained

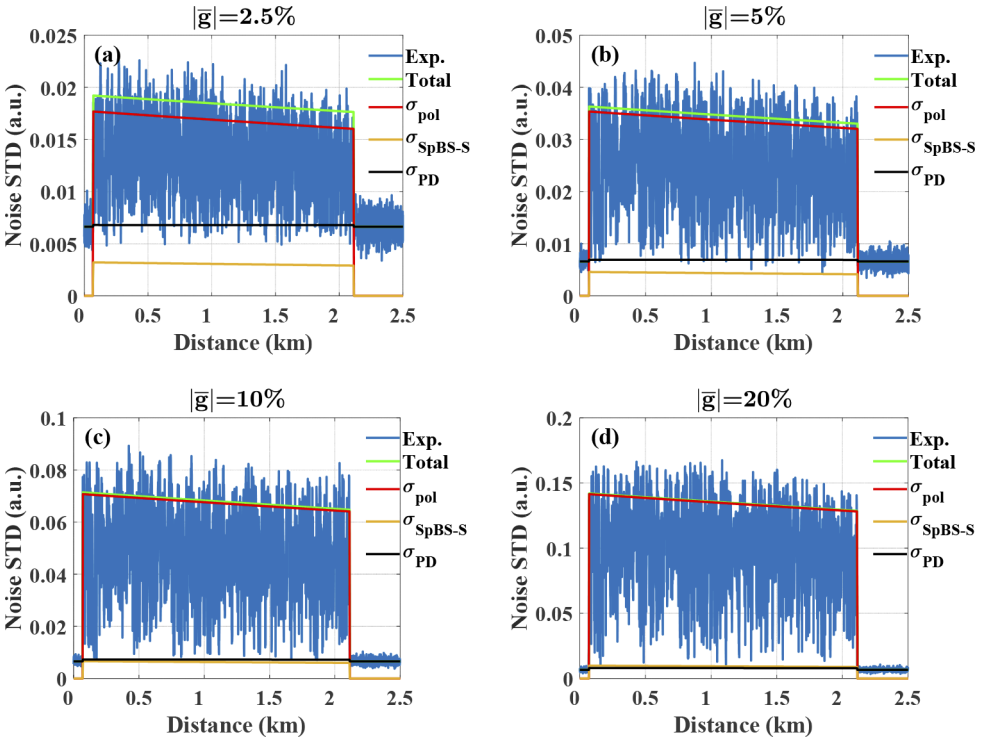

Fig. 3. Noise distribution at the Brillouin resonance peak along a 2 km sensing fiber for (a) $|\bar{g}| = 2.5\%$; (b) $|\bar{g}| = 5\%$; (c) $|\bar{g}| = 10\%$; (d) $|\bar{g}| = 20\%$.

Optics EXPRESS

SOP transitions, and the maximum value of STDs is the most meaningful. Experimental results match well with the theoretically calculated STDs (green curves) in all cases, demonstrating the correctness of the equations established previously in this section. This also verifies the fact that, for long-range sensing, the optical noise impacts more at the fiber near-end (where $|\overline{g(z)}|$ may reach a few percent) and shows negligible impact at the fiber far-end (where $|\overline{g(z)}|$ is typically orders of magnitude smaller than 1%), as evidenced in [21].

3. Noise analysis of a coded BOTDA system

By contrast with the aforementioned single-pulse system, the probe wave is amplified by tens of pump pulses along a single trace in unipolar-coded BOTDA, resulting in a much larger net Brillouin gain, e.g. ~100% at the fiber near-end in fully optimized cases [23]. This leads to significantly enhanced Brillouin-gain-dependent noises, which may result in a significant reduction of the actual coding gain with respect to the expected theoretical value, being the latter calculated by assuming that the noise level is unchanged from the single-pulse BOTDA to the unipolar-coded BOTDA. In this section, noises in unipolar-coded BOTDA are studied, aiming at figuring out the actual coding gain at any fiber position under a given experimental condition, thus rigorously evaluating the real benefit provided by a given coded-BOTDA system.

The model is based on the standard setup for unipolar-coded BOTDA [23], in which a polarization scrambler is used to alleviate the impact of polarization fading and pulling. In this case the photocurrent of the detected optical signal at the n^{th} acquisition is similar to Eq. (1), with a net Brillouin gain expressed as:

$$G(z,n) = \sum_{i=1}^{L_C} 2\overline{g(z)}C_i\cos^2\theta(i,z,n), \tag{7}$$

where L_C and C_i denote the code bit number and the state (either 0 or 1) of the i^{th} coded pulse, respectively, $\theta(i,z,n)$ is the relative polarization angle between the i^{th} coded pulse and the probe wave, which is randomly distributed over the range $[0,\pi]$. Based on Eq. (7) and following the similar derivation procedure for Eqs. (4)–(6), noises in the coded-BOTDA are modelled as:

1) *Polarization noise*. Since $G(z,n)$ results from all coded pulses interacting with the probe wave at different fiber locations, each coded pulse suffers from different levels of polarization noise, depending on the aforementioned SOP transitions. Taking this statistical effect into account, the polarization noise STD in coding systems can be expressed as (see detailed derivation in Appendix):

$$\sigma^C_{Pol}(z) = K\sqrt{\langle G(z,n)^2\rangle_n - \langle G(z,n)\rangle_n{}^2} \approx \frac{K|\overline{G(z)}|}{\sqrt{2M}}, \tag{8}$$

where K=0.67 is a scaling factor estimating the statistics of the SOP transitions, obtained by calculating the square root of the ratio between the average variance and maximum variance of the trace in Fig. 1(a). As will be demonstrated later, this characterization of K leads to good results for all noise estimations, since they match well with all experimental data presented hereafter. In Eq. (8), $\overline{G(z)}$ is the mean coded Brillouin gain at the Brillouin resonance peak, i.e., $\overline{G(z)} = \mathrm{G}(z,n)_n = M\overline{g(z)}$, where M is the number of '1' elements in the coded pulses.

2) *SpBS-Signal beating noise.* Similar to Eq. (5), the noise STD can be expressed as:

$$\sigma^C_{SpBS-S}(z) = \frac{\sqrt{\overline{E^2_{SpBS}(z)E^2_S(z)}}}{P^0_S\exp[\overline{G(z)}]} = \sqrt{\frac{P^C_{SpBS}(z)}{P^0_S\exp[\overline{G(z)}]}} \propto \sqrt{\frac{|\overline{G(z)}|}{P^0_S\exp[\overline{G(z)}]}}, \tag{9}$$

Optics EXPRESS

where $P^C_{SpBS}(z) = MP^S_{SpBS}(z)$ representing the power of SpBS originating from the coding sequence, i.e., the summation of SpBS attributed to each coded pulse.

3) *Photo-detection noise,* expressed as:

$$\sigma^C_{PD}(z) \approx \frac{\sigma_{th}}{\eta P^0_S \exp[\overline{G(z)}]}. \tag{10}$$

From Eqs. (8)–(10) it can be found that, the key parameter determining all noises is the mean coded Brillouin gain $\overline{G(z)}$, whose characteristic differs depending on the given code type. For aperiodic codes such as Simplex [13], Golay [12] and GO-code [16], $|\overline{G(z)}|$ decays exponentially from the fiber near-end to the far-end due to the fiber loss, i.e., decays from $|\overline{G(0)}|$ that should be ideally around 100% [16,23] to $|\overline{G(end)}|$ that equals to $|\overline{G(0)}|\exp(-\alpha z)$, where α is the fiber loss coefficient in linear scale. For instance, with a 50 km sensing range, the value of $|\overline{G(end)}|$ turns out to be around 10%.

On the other hand, for periodic codes such as cyclic codes, in which the coded pulses sparsely spread over the entire fiber length, $|\overline{G(z)}|$ remains similar at any fiber position [14], so that $|\overline{G(z)}| \approx |\overline{G(0)}| \approx |\overline{G(end)}|$. Note that such an equality holds only when the pulse separation is sufficiently short to neglect the impact of fiber losses between the responses to each pulse, which normally matches the real situation. In Eq. (8), apart from $|\overline{G(z)}|$, the number of '1' elements, M, also determines the amount of polarization noise. In general, M should be maximized to maximize the theoretical coding gain $\sqrt{M/2}$; however, M is practically limited by higher-order nonlocal effects [23], such that the wider the spatial resolution, the smaller the maximum allowable M (e.g., M must be around 40 for 2 m spatial resolution for optimal conditions).

Figures 4(a) and (b) illustrates the theoretically calculated noise STD as a function of $|\overline{G(z)}|$, for M = 32 and 64, respectively. In both figures, $|\overline{G(z)}|$ ranges from 0 to 100%, covering most possible $|\overline{G(z)}|$ for both periodic and aperiodic codes, thus sufficient to investigate the noise behavior at any fiber position for any existing code type. Figures intuitively show that, 1) when $|\overline{G(z)}|$ is larger than ~10%, the optical noise (including polarization noise and SpBS-signal beating noise) dominates over the thermal noise, compromising the theoretical coding gain ($\sqrt{M/2}$) that only considers the thermal noise; 2) The larger the M, the smaller the total noise. Results indicate that, for aperiodic codes, the theoretical coding gain is compromised at the fiber near-end where $|\overline{G(z)}|$ is large, which however may be reached at the fiber far-end where $|\overline{G(z)}|$ is small. On the other hand, for periodic codes, the theoretical coding gain is always compromised at any fiber position, due to the uniformly large $|\overline{G(z)}|$ over the entire fiber.

Experiments using Simplex code (aperiodic) and cyclic Simplex code (periodic) based on the typical unipolar-coded BOTDA setup [23] are carried out to demonstrate the above analysis. A 50 km-long single-mode optical fiber is used as the sensing fiber, which is formed by two ~25 km fiber spools with similar BFS. In the experiment, all time-domain traces are detected by a PD with a 3 dB bandwidth of 75 MHz, and relevant decoding process is performed on each normalized trace without post-processing filtering. In all cases, the optical power of the continuous-wave probe P^0_S reaching the photodetector is set to -20 dBm, which is just below the PD saturation.

First, the noise model expressed by Eqs. (8)–(10) is verified with Simplex code. Figures 5(a) and (b) show the noise STD profiles as a function of distance (blue curves), computed from 20 consecutive measurements with no trace average, for M = 32 and 64, respectively. Theoretical profiles (green, red, yellow and black curves) predicted by Eqs. (8)–(10) are also plotted, in which the total noise is in good agreement with measurements. Results also verify that, at the fiber near-end optical noises (red and yellow curves) dominate, while near the fiber far-end the detection thermal noise (black curve) dominates as the optical noises are highly reduced due to fiber loss.

Optics EXPRESS

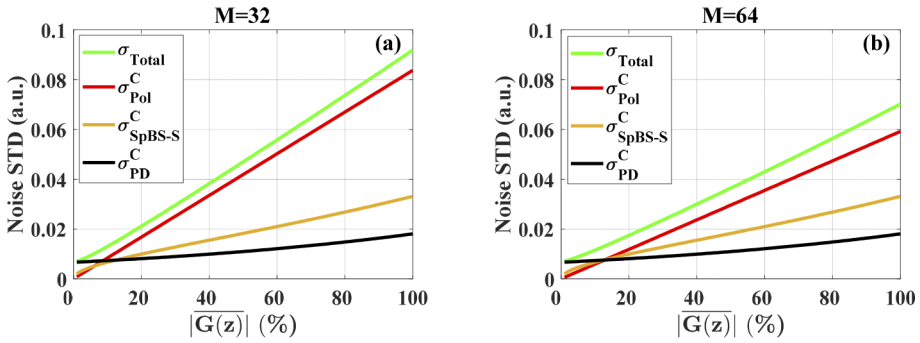

Fig. 4. STD of noises as a function of $|\overline{G(z)}|$ for (a) $M = 32$; (b) $M = 64$. Relevant parameters are: $K = 0.67$; $\alpha_{SpBS} = -93$ dB/m; The photodetector responsivity η and conversion gain are 1 A/W and 150000 V/A, respectively. $P_S^0 = -20$ *dBm*.

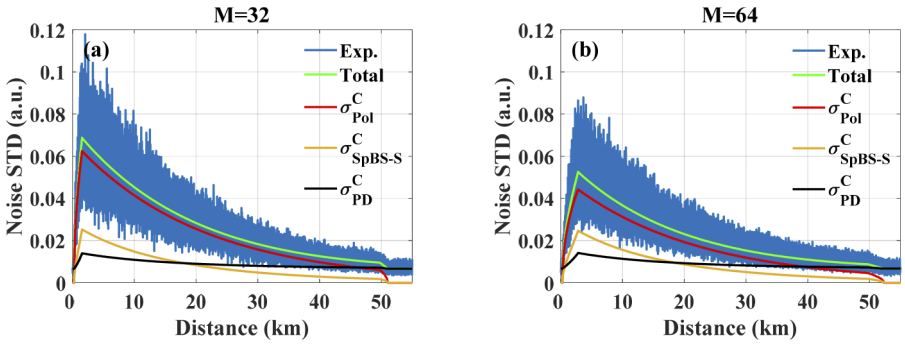

Fig. 5. STD of 20 consecutive noises obtained without averaging over 50 km fiber for (a) $M = 32$; (b) $M = 64$.

Then, the actual coding gain at each fiber position using Simplex code and cyclic Simplex code is investigated by comparing the attained SNR and BFS with the ones obtained by the optimized single-pulse BOTDA. The spatial resolution is set to 2 m, corresponding to an optimized mean single-pulse Brillouin gain $|\overline{g(0)}|$ of 2.5%. In both coded-BOTDA schemes, the power of each coded pulse is adjusted to be equal to that of the optimized single pulse. In the case of Simplex coded system, a 63-bit code length (M=32) is used, corresponding to a theoretical coding gain of 6 dB ($= 10\log_{10}\left(\sqrt{32/2}\right)$). To perform a fair comparison, in the case of cyclic Simplex code a 67-bit code length ($M = 34$) is used, corresponding to a theoretical coding gain of 6.2 dB ($= 10\log_{10}\left(\sqrt{34/2}\right)$), close to that of the aperiodic Simplex code.

The STD of noises as well as the theoretical predictions for single-pulse case and both codes are shown in Figs. 6(a) and (b), all obtained without averaging. It can be noticed that the noise in the case of cyclic code is globally higher than the noise in the single-pulse case. Figures 6(c) and (d) show SNRs of the single-pulse case and both codes after decoding, all obtained with around 1024 averages for the sake of visual clarity (16 avgs × 63 traces for aperiodic Simplex code, and 1024 avgs × 1 trace for both single-pulse case and cyclic Simplex code). In the case of aperiodic Simplex code (Fig. 6(c)), the actual coding gain (i.e., the SNR improvement compared to the single pulse case) at the fiber near-end is -1.23 dB due to the large optical noises, and at the fiber far-end is 5 dB, which is only 1 dB lower than the theoretical coding gain (6 dB). On the other hand, cyclic code can nearly bring no coding gain (see Fig. 6(d)), which seems to contradict

Optics EXPRESS

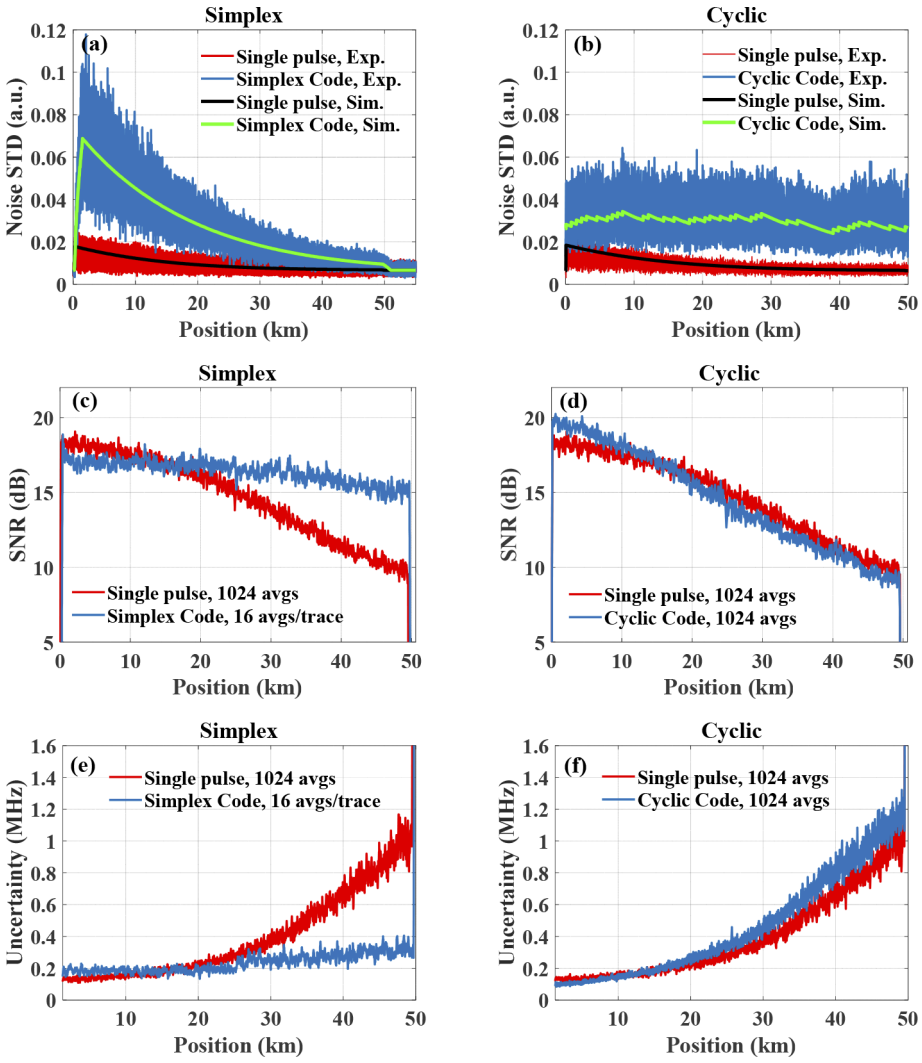

Fig. 6. Comparison between optimized single-pulse BOTDA and coded BOTDA, using an optimized peak pump power of 100 mW. Noise STD obtained by 20 consecutive measurements without averaging, over a 50 km fiber, for (a) a 63 bits aperiodic Simplex coded system and (b) a 67 bits cyclic Simplex system. SNR profiles at the Brillouin resonance peak for (c) 63 bits aperiodic Simplex coded system and (d) 67 bits cyclic Simplex system. BFS uncertainty profiles along the 50 km fiber for (e) 63 bits aperiodic Simplex coded system and (f) 67 bits cyclic Simplex system.

with results reported in some literature (e.g., [27]) where the theoretical coding gain of cyclic Simplex code was successfully realized. Note that such a demonstration was due to the use of non-optimized pulse peak power, in both single-pulse and cyclic Simplex coding schemes (i.e. using 16 mW in [27], being 10 times below the MI threshold), such that the signal-dependent optical noises are much lower, making the attained coding gain to be close to the theoretical value. However, improving the measurement SNR under such a suboptimal condition is of limited overall impact, since the absolute SNR obtained with cyclic coding in suboptimal cases could be even lower than the one obtained in an optimized single-pulse scheme, nullifying the meaning of

Optics EXPRESS

using pulse coding to enhance the performance of BOTDA sensors. Finally, BFS uncertainty profiles along the fiber, estimated by taking the STD of BFS profiles obtained by 5 consecutive measurements, are shown in Figs. 6(e) and (f). In the case of aperiodic Simplex code, the BFS uncertainty obtained at the fiber far-end by the Simplex code scheme (0.35 MHz) is about 3 times better than the one obtained by the single-pulse scheme (1 MHz), in good agreement with the evaluated coding gain (5 dB). While in the case of cyclic coding, the BFS uncertainty is slightly higher than the one obtained by an optimized single-pulse scheme, indicating that there is no benefit brought by cyclic coding when comparing with a fully optimized single-pulse scheme.

To better show the performance difference between periodic and aperiodic codes, Figs. 7(a) and (b) illustrate the coding gains as a function of M for both codes when the spatial resolution is 2 m and 1 m, respectively. In both figures, black lines denote the reference coding gain that are theoretically calculated as $\sqrt{M/2}$, red lines and blue lines denote the actual coding gains of aperiodic and periodic codes, respectively. Results consolidate the fact that aperiodic codes always outperform periodic codes for any value of M.

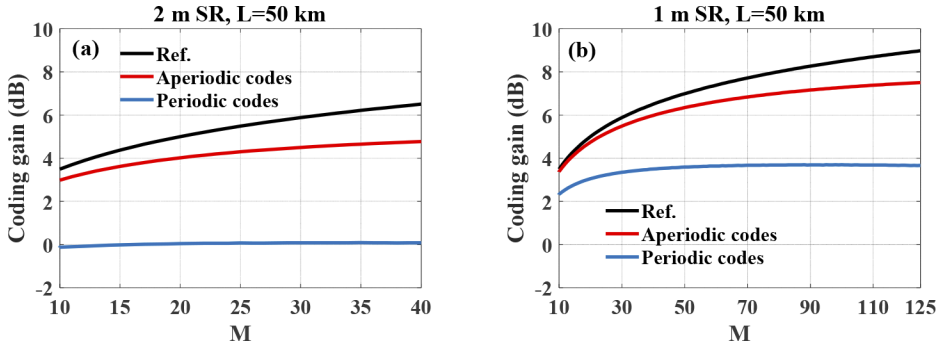

Fig. 7. Coding gains as a function of M for both aperiodic and periodic codes when the spatial resolution is (a) 2 m and (b) 1 m, respectively.

4. Conclusion

In this paper, noise models for both single-pulse and coded BOTDA have been theoretically established and experimentally validated, enabling to predict the coding gain at any fiber location using any code type for any given experimental condition. Based on the noise models, the reported analysis points out that the Brillouin-gain-dependent optical noises, such as polarization noise and SpBS-signal beating noise, could highly compromise the attained coding gain that is theoretically defined by assuming that the noise level of the coded BOTDA system remains unchanged with respect to the single-pulse BOTDA. The impact of such noises differs depending on the code type:

1) For aperiodic codes, the coding gain is always largely compromised at the fiber near-end due to the large Brillouin gain, while at the fiber far-end the local Brillouin gain reduces due to the fiber attenuation, so that the penalty of coding gain due to optical noises partially or entirely vanishes depending on the fiber length. This feature makes aperiodic pulse coding effectively enhance the SNR and performance of long-range BOTDA sensors, especially at the end of long fibers, where normally thermal noise dominates the measurements.

2) For periodic codes, optical noises remain globally strong over the entire measured time-domain trace (i.e. along the entire fiber length), nullifying the benefit of coding at any fiber location. Note however that, for a non-optimized pulse power, cyclic coding can

Optics EXPRESS

be effective as demonstrated by previous publications, though this condition has not yet proved to bring any global advantage in real conditions.

It is expected that the model could serve as a useful tool to optimize the performance of coded-BOTDA sensors by trading-off the number of code words and the noise. In addition, similar procedure and strategies can be derived for analyzing the impact of noises on BOTDA using other code types. For instance, based on Eqs. (8)–(10) it can be readily predicted that the polarization noise would be much smaller in the case of color-coded BOTDA [17], because of the smaller $\overline{G(z)}$ attributed to coded pulses with different frequencies. It can also be expected that the polarization noise is extremely small in bipolar-coded BOTDA [19], as '+1' and '-1' elements would result in a $\overline{G(z)}$ similar to that of a single pulse, yielding a much higher SNR improvement than unipolar codes. All above analysis also implies that technologies based on distributed Raman amplification (DRA) [28,29], in which $\overline{G(z)}$ keeps being the same level as the single-pulse Brillouin gain, is also a good avenue to improve the SNR, provided that the relative intensity noise (RIN) [30,31] resulting from the Raman amplification can be effectively eliminated.

Appendix

This appendix shows the detailed derivations from the expression of coded Brillouin gain (Eq. (7)) to the expression of polarization noise STD (Eq. (8)).

First, considering the fact that all '0' elements in the coded sequence do not contribute to the net Brillouin gain $G(z,n)$, we rewrite Eq. (7) to only consider the contribution of '1' elements as:

$$G(z,n) = \sum_{p=1}^{M} 2\overline{g(z)}\cos^2\theta(p,z,n), \tag{11}$$

where M is the number of '1' elements, and p is the index of each '1' element after removing all '0' elements in the coded sequence. Substitute Eq. (11) into the following expression that calculates the STD of $G(z,n)$ over n acquisitions:

$$\sigma_G^C(z) = \sqrt{\left\langle G(z,n)^2\right\rangle_n - \langle G(z,n)\rangle_n{}^2}, \tag{12}$$

where the term $\langle \mathrm{G}(z,n)\rangle^2{}_n$ can be calculated as:

$$\begin{aligned}\left\langle G(z,n)^2\right\rangle_n &= \left\langle [2\overline{g(z)}\cos^2\theta(1,z,n) + 2\overline{g(z)}\cos^2\theta(2,z,n) + \cdots 2\overline{g(z)}\cos^2\theta(M,z,n)]^2\right\rangle_n \\ &= 4M\overline{g(z)}^2\left\langle\cos^4\theta(p,z,n)\right\rangle_n + 4M(M-1)\overline{g(z)}^2\left\langle\cos^2\theta(p,z,n)\cos^2\theta(q,z,n)\right\rangle_n,\end{aligned} \tag{13}$$

where $\theta(p,z,n)$ and $\theta(q,z,n)$ are the relative polarization angles between probe wave and the p^{th} coded '1' pulse and the q^{th} coded '1' pulse, respectively, which are statistically independent and randomly distributed in the range $[0,\pi]$ for each acquisition number n. Knowing that the following mathematical relations: $\left\langle cos^2\theta(p,z,n)cos^2\theta(q,z,n)\right\rangle_n = \left\langle cos^2\theta(p,z,n)\right\rangle_n \cdot \left\langle cos^2\theta(q,z,n)\right\rangle_n = 1/4$, and $cos^4\theta(p,z,n)_n = 3/8$, Eq. (13) can be simplified as:

$$\left\langle G(z,n)^2\right\rangle_n = \frac{1}{2}M\overline{g(z)}^2 + M^2\overline{g(z)}^2. \tag{14}$$

Then, the other term in Eq. (12), $\langle \mathrm{G}(z,n)_n{}^2\rangle$, can be calculated as:

$$\langle G(z,n)\rangle_n{}^2 = \left[2M\overline{g(z)}\left\langle\cos^2\theta(p,z,n)\right\rangle_n\right]^2 = M^2\overline{g(z)}^2. \tag{15}$$

Optics EXPRESS

Substituting Eqs. (14) and (15) into Eq. (12), the following expression for the STD of $G(z, n)$ can be obtained:

$$\sigma_G^C(z) = \sqrt{\frac{1}{2}M\overline{g(z)}^2 + M^2\overline{g(z)}^2 - M^2\overline{g(z)}^2} = \sqrt{\frac{1}{2}M\overline{g(z)}^2} = \frac{M|\overline{g(z)}|}{\sqrt{2M}} = \frac{|\overline{G(z)}|}{\sqrt{2M}}. \quad (16)$$

Finally, taking into account the scaling factor K that estimates the statistics of the SOP transitions as explained in the main text, the polarization noise STD in coded BOTDA can be expressed as Eq. (8) in the main text.

Funding. National Natural Science Foundation of China (61875018); Innosuisse Innovation Project (38390.1); ANID Chilean National Agency for Research and Development, Basal Project (FB0008); Fondecyt Regular (1200299).

Disclosures. The authors declare that there are no conflicts of interest related to this article.

Data availability. Data underlying the results presented in this paper are not publicly available at this time but may be obtained from the authors upon reasonable request.

References

1. A. H. Hartog, An introduction to distributed optical fibre sensors (CRC, 2017).
2. T. Horiguchi, K. Shimizu, T. Kurashima, M. Tateda, and Y. Koyamada, "Development of a distributed sensing technique using Brillouin scattering," J. Lightwave Technol. **13**(7), 1296–1302 (1995).
3. A. Motil, A. Bergman, and M. Tur, "State of the art of Brillouin fiber-optic distributed sensing," Opt. Laser Technol. **78**, 81–103 (2016).
4. M. A. Soto, *Distributed Brillouin Sensing: Time-Domain Techniques*, (Springer Nature Publishers, 2018).
5. M. A. Soto and L. Thévenaz, "Modeling and evaluating the performance of Brillouin distributed optical fiber sensors," Opt. Express **21**(25), 31347–31366 (2013).
6. S. M. Foaleng, F. Rodríguez-Barrios, S. Martin-Lopez, M. Gonzalez-Herraez, and L. Thévenaz, "Detrimental effect of self-phase modulation on the performance of Brillouin distributed fiber sensors," Opt. Lett. **36**(2), 97–99 (2011).
7. M. Alem, M. A. Soto, and L. Thévenaz, "Analytical model and experimental verification of the critical power for modulation instability in optical fibers," Opt. Express **23**(23), 29514–29532 (2015).
8. D. Cotter, "Observation of stimulated Brillouin scattering in low-loss silica fibre at 1.3 μm," Electron. Lett. **18**(12), 495–496 (1982).
9. L. Thévenaz, S. F. Mafang, and J. Lin, "Effect of pulse depletion in a Brillouin optical time-domain analysis system," Opt. Express **21**(12), 14017–14035 (2013).
10. A. Domínguez-López, X. Angulo-Vinuesa, A. López-Gil, S. Martín-López, and M. González-Herráez, "Nonlocal effects in dual-probe-sideband Brillouin optical time domain analysis," Opt. Express **23**(8), 10341–10352 (2015).
11. S. Zaslawski, Z. Yang, and L. Thévenaz, "On the 2D Post-Processing of Brillouin Optical Time-Domain Analysis," J. Lightwave Technol. **38**(14), 3723–3736 (2020).
12. M. Nazarathy, S. A. Newton, R. P. Giffard, D. S. Moberly, F. Sischka, W. R. Trutna, and S. Foster, "Real-time long range complementary correlation optical time domain reflectometer," J. Lightwave Technol. **7**(1), 24–38 (1989).
13. D. Lee, H. Yoon, P. Kim, J. Park, and N. Park, "Optimization of SNR improvement in the noncoherent OTDR based on simplex codes," J. Lightwave Technol. **24**(1), 322–328 (2006).
14. M. A. Soto, T. Nannipieri, A. Signorini, A. Lazzeri, F. Baronti, R. Roncella, and F. Di Pasquale, "Raman-based distributed temperature sensor with 1 m spatial resolution over 26 km SMF using low-repetition-rate cyclic pulse coding," Opt. Lett. **36**(13), 2557–2559 (2011).
15. H. Iribas, A. Loayssa, F. Sauser, M. Llera, and S. Le Floch, "Cyclic coding for Brillouin optical time-domain analyzers using probe dithering," Opt. Express **25**(8), 8787–8800 (2017).
16. X. Sun, Z. Yang, X. Hong, S. Zaslawski, S. Wang, M. A. Soto, X. Gao, J. Wu, and L. Thévenaz, "Genetic-optimised aperiodic code for distributed optical fibre sensors," Nat. Commun. **11**(1), 1–11 (2020).
17. S. Le Floch, F. Sauser, M. Llera, M. A. Soto, and L. Thévenaz, "Colour simplex coding for Brillouin distributed sensors," *Proc. SPIE 8794, Fifth European Workshop on Optical Fibre Sensors (EWOFS)*, 879437 (2013).
18. S. L. Floch, F. Sauser, M. Llera, and E. Rochat, "Novel Brillouin Optical Time-Domain Analyzer for Extreme Sensing Range Using High-Power Flat Frequency-Coded Pump Pulses," J. Lightwave Technol. **33**(12), 2623–2627 (2015).
19. Z. Yang, M. A. Soto, and L. Thévenaz, "Increasing robustness of bipolar pulse coding in Brillouin distributed fiber sensors," Opt. Express **24**(1), 586–597 (2016).
20. J. Urricelqui, M. A. Soto, and L. Thévenaz, "Sources of noise in Brillouin optical time-domain analyzers," *24th International Conference on Optical Fibre Sensors*, 9634, 963434 (2015).
21. S. Wang, Z. Yang, M. A. Soto, and L. Thévenaz, "Study on the signal-to-noise ratio of Brillouin optical-time domain analyzers," Opt. Express **28**(14), 19864–19876 (2020).
22. M. A. Soto, M. Tur, A. Lopez-Gil, M. Gonzalez-Herraez, and L. Thévenaz, "Polarisation pulling in Brillouin optical time-domain analysers," Proc. SPIE **10323**, 103239L (2017).
23. Z. Yang, Z. Li, S. Zaslawski, L. Thévenaz, and M. A. Soto, "Design rules for optimizing unipolar coded Brillouin optical time-domain analyzers," Opt. Express **26**(13), 16505–16523 (2018).

Optics EXPRESS

24. Y. Zhou, L. Yan, Z. Li, W. Pan, and B. Luo, "Polarization division multiplexing pulse coding for eliminating the effect of polarization pulling in Golay-coded BOTDA fiber sensor," Opt. Express **26**(15), 19686–19693 (2018).
25. M. O. Van Deventer and A. J. Boot, "Polarization properties of stimulated Brillouin scattering in single-mode fibers," J. Lightwave Technol. **12**(4), 585–590 (1994).
26. B. E. A. Saleh and M. C. Teich, *Fundamentals of Photonics*, (John Wiley & Sons, 1991), Chap. 17.
27. M. Taki, Y. Muanenda, C. J. Oton, T. Nannipieri, A. Signorini, and F. Di Pasquale, "Cyclic pulse coding for fast BOTDA fiber sensors," Opt. Lett. **38**(15), 2877–2880 (2013).
28. F. Rodríguez-Barrios, S. Martín-López, A. Carrasco-Sanz, P. Corredera, J. D. Ania-Castañón, L. Thévenaz, and M. González-Herráez, "Distributed Brillouin fiber sensor assisted by first-order Raman amplification," J. Lightwave Technol. **28**(15), 2162–2172 (2010).
29. M. A. Soto, G. Bolognini, and F. Di Pasquale, "Optimization of long-range BOTDA sensors with high resolution using first-order bi-directional Raman amplification," Opt. Express **19**(5), 4444–4457 (2011).
30. X. Angulo-Vinuesa, A. Dominguez-Lopez, A. Lopez-Gil, J. D. Ania-Castañón, S. Martin-Lopez, and M. Gonzalez-Herraez, "Limits of BOTDA range extension techniques," IEEE Sens. J. **16**(10), 3387–3395 (2016).
31. A. Domínguez-López, A. López-Gil, S. Martín-López, and M. González-Herráez, "Strong cancellation of RIN transfer in a Raman-assisted BOTDA using balanced detection," IEEE Photon. Technol. Lett. **26**(18), 1817–1820 (2014).